

Neural network approach for the dynamics on the normally hyperbolic invariant manifold of periodically driven systems

Martin Tschöpe,¹ Matthias Feldmaier,¹ Jörg Main,¹ and Rigoberto Hernandez^{2,*}

¹*Institut für Theoretische Physik 1, Universität Stuttgart, 70550 Stuttgart, Germany*

²*Department of Chemistry, Johns Hopkins University, Baltimore, Maryland 21218, USA*

(Dated: October 27, 2021)

Chemical reactions in multidimensional systems are often described by a rank-1 saddle, whose stable and unstable manifolds intersect in the normally hyperbolic invariant manifold (NHIM). Trajectories started on the NHIM in principle never leave this manifold when propagated forward or backward in time. However, the numerical investigation of the dynamics on the NHIM is difficult because of the instability of the motion. We apply a neural network to describe time-dependent NHIMs and use this network to stabilize the motion on the NHIM for a periodically driven model system with two degrees of freedom. The method allows us to analyze the dynamics on the NHIM via Poincaré surfaces of section (PSOS) and to determine the transition state (TS) trajectory as a periodic orbit with the same periodicity as the driving saddle, viz. a fixed point of the PSOS surrounded by near-integrable tori. Based on Transition State Theory and a Floquet analysis of a periodic TS trajectory we compute the rate constant of the reaction with significantly reduced numerical effort compared to the propagation of a large trajectory ensemble.

I. INTRODUCTION

In chemical reactions, the precise separation between reactants and products is a key to determining rate constants. Usually, the boundary between these regions contains an energetic barrier in phase space—typically a rank-1 saddle—to which an appropriate dividing surface (DS) can be associated or attached. Transition State Theory (TST) [1–18] uses the particle flux through a DS to determine the rate of a chemical reaction.

For an exact reaction rate, it is crucial to have a *recrossing-free* DS because recrossings would lead to an overestimation of the rate otherwise. The major importance of the TST follows from the broad variety of fields, where it can be applied to, including for instance atomic physics [19], solid state physics [20], cluster formation [21, 22], diffusion dynamics [23, 24], cosmology [25], celestial mechanics [26, 27], and Bose-Einstein condensates [28–32], to name a few. For *time-dependent* systems, e.g. subject to periodical driving due to external fields, the situation becomes more challenging. Here, the DS itself becomes time-dependent and depends non-trivially on the saddle of the potential. The DS can nevertheless be obtained, e.g., by using a minimization procedure based on the Lagrangian descriptors (LDs) [33–36].

In a system with d degrees of freedom, the time-dependent DS embedded in phase space has dimension $2d - 1$ and is attached to the $(2d - 2)$ -dimensional normally hyperbolic invariant manifold (NHIM), which has the property that every trajectory on the NHIM will never leave this manifold. In a periodically driven system, we can construct and define a transition state (TS) trajectory which never escapes from the reactant region and which is a periodic orbit with the same period as

the driving potential [37–46]. In the limit of a system with one degree of freedom, the NHIM reduces to a point moving along the TS trajectory. However, in systems with two or more degrees of freedom the structure of the NHIM and the dynamics of trajectories on it becomes non-trivial. Slowly reacting particles spend a longer time in the vicinity of the NHIM crossing the DS closer to the NHIM, and therefore the dynamics on the NHIM is of special interest [47].

In this paper, we focus on the numerical determination of the dynamics on the NHIM of a periodically driven system with more than one degree of freedom. Because of the unstable degree of freedom, trajectories on the NHIM tend to separate exponentially fast from this manifold. This makes it difficult, if not impossible, to investigate numerically the long-time behavior of the dynamics. Here, we present a method that prevents numerically determined trajectories from leaving the NHIM by approximating the NHIM with a neural network (NN) and stabilizing the dynamics onto the NHIM. NNs have already found use in molecular dynamics [48], and have been seen to be a powerful tool in the computation of potential energy surfaces [49–58] and the construction of the DSs [36, 59].

The challenge, addressed in this paper, is the determination of the dynamics of trajectories within the NHIM for systems with two or more degrees of freedom. This is challenging because trajectories in the neighborhood of the NHIM are unstable and depart exponentially fast from it. Applying NNs to stabilize the trajectories on the NHIM allows us to analyze them numerically using the tools of nonlinear dynamics and thereby determine dynamical properties such as reaction rates. To illustrate the former, the dynamics on the NHIM has been resolved in this work using a stroboscopic Poincaré surface of section (PSOS).

For a periodically driven model system with two degrees of freedom we show that the dynamics on the NHIM

* Correspondence to: r.hernandez@jhu.edu

is governed by torus-like structures with a fixed point at its center representing a periodic orbit with the same period as the driving potential. We define this orbit as a periodic TS trajectory in analogy to systems with one degree of freedom. We have developed two methods, a centroid and a friction search algorithm, to numerically extract such a TS trajectory in multidimensional systems.

Of particular importance is the question as to whether rate constants of chemical reactions can be manipulated by periodic driving of the system. Rate constants can be obtained from appropriately chosen ensembles of trajectories by evaluating the time-dependent number of reactive trajectories having crossed the DS [35, 36]. In Ref. 42 a Floquet analysis is used instead of ensemble propagation to obtain the rate constant in a one-dimensional, periodically driven model system with a moving saddle. We generalize and apply the Floquet analysis to a periodic TS trajectory of the model system with two degrees of freedom obtained with either the centroid search or the friction search and show that the rate constants computed with this method are in excellent agreement with numerically much more expensive ensemble calculations.

Thus the central results of this paper are (i) the demonstration of NNs for determining the multidimensional — viz in 2 dimensions — dynamics of the NHIM, and (ii) the demonstration that detailed knowledge of the dynamics on the NHIM, stabilized by NNs, can be used to extend the one-dimensional Floquet method introduced in Ref. 42 to obtain rate constants in systems with two or more degrees of freedom.

The paper is organized as follows. In Sec. II we introduce the theory and methods to apply a NN for the construction of the time-dependent NHIM, the stabilization of the dynamics on the NHIM, and the computation of rate constants. In Sec. III results demonstrating the efficacy and efficiency of NNs for determining rate constants are presented and discussed. We conclude in Sec. IV that our new approaches do indeed provide accurate and more efficient determinations of the rates of driven reactions at increasingly higher dimensionality.

II. THEORY AND METHODS

In Sec. IIA we start with the definition and physical fundamentals of the normally hyperbolic invariant manifold (NHIM) including its numerical construction, and give a short overview of neural networks (NNs), used in Sec. IIB to stabilize the dynamics on the NHIM. In Sec. IIC we then discuss the Floquet analysis for the transition state (TS) trajectory and its application to determine rate constants of the system with significantly reduced numerical effort compared to methods based on the propagation of trajectory ensembles.

A. Construction of the time-dependent NHIM

We consider a system with d degrees of freedom, where the reactants and products are separated by a time-dependent potential barrier given by a rank-1 saddle. A particle reacts, when it overcomes the saddle from one basin to the other along the reaction coordinate x . The remaining $d-1$ coordinates \mathbf{y} are called bath coordinates [36]. The reaction pathways and the corresponding reaction rate of the system are determined by the local properties of the barrier. The normally hyperbolic invariant manifold (NHIM) is the $(2d-2)$ -dimensional manifold in the $(2d)$ -dimensional phase space which contains all trajectories that are trapped in the saddle region both forward and backward in time. Since we consider time-dependent systems, the NHIM is in general also time-dependent. The dynamics on the NHIM is of special interest for the reaction dynamics, for the reason that the slower a particle reacts, the more it is influenced by the saddle and the closer it passes the NHIM.

A prerequisite for the investigation of the dynamics on the NHIM is the numerical construction and efficient description of this manifold. This aim can be achieved in two steps: In a first step, we compute a small number of individual points

$$\begin{aligned} x^{\text{NHIM}} &= x^{\text{NHIM}}(\mathbf{y}, \mathbf{v}_y, t), \\ v_x^{\text{NHIM}} &= v_x^{\text{NHIM}}(\mathbf{y}, \mathbf{v}_y, t) \end{aligned} \quad (1)$$

on the NHIM depending on the bath coordinates, velocities, and time. Each of these points corresponds to a point on one of the bound trajectories to the NHIM, captured at a particular time t . The stable and unstable manifolds $\mathcal{W}_{s,u}$ play an important role in this picture. Here, the stable manifold \mathcal{W}_s is the set of points that approach the NHIM exponentially fast, and the unstable manifold \mathcal{W}_u consists of those points that depart exponentially fast from the NHIM. The points $(x^{\text{NHIM}}, v_x^{\text{NHIM}})$ in Eq. (1) are given as the intersection of the stable and unstable manifolds $\mathcal{W}_{s,u}$, and can be numerically determined by application of the binary contraction method [36, 60]. This two-dimensional bisection method can be used to obtain individual points on the NHIM to high precision. However, this comes at the cost of computation time because it requires the propagation of a large number of trajectories.

In a second step, the high-accuracy points obtained in the first step are used for the training of a neural network (NN) as discussed in Refs. 36 and 59 that allows for the numerically fast and efficient interpolation to an effectively continuous set of points on the NHIM. Any candidate trajectory can then be analyzed relative to the NN NHIM to determine if it is reactive. It can also be used to determine rates directly as shown below.

For the convenience of the reader, we here briefly recapitulate the basic ideas of NNs. The more interested reader is referred to the literature, *e.g.*, Refs. 61 and 62. In general, a NN consists of *layers* which can each

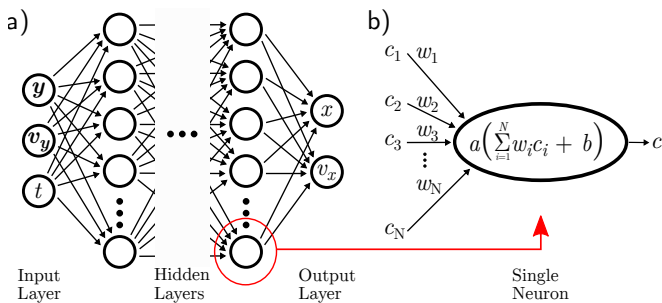


FIG. 1. Basic construction of a feed-forward neural network (a) and an individual neuron (b). Here, we use such networks for the multidimensional regression task of interpolating the $(2d - 2)$ -dimensional NHIM of a $(2d)$ -dimensional, time-dependent system. For any given time t , the reaction coordinates (x, v_x) are continuously obtained using the network with the $(2d - 2)$ phase space coordinates $(\mathbf{y}, \mathbf{v}_y)$ and the time t as input. The weights w and the biases b are obtained using the *Adam optimizer* (see text).

be represented as a vector in a mathematical sense, see Fig. 1(a). Every layer is composed of *neurons*, which correspond to the entries of the vector and are represented in Fig. 1(b). A simple form of NNs is a *feed-forward* neural net in which information propagates only in one direction. The values for the $(l + 1)$ -st layer are obtained as follows:

1. Multiply the l -th *weight matrix* w_{ij} with the values of the l -th layer $c_j^{(l)}$.
2. Add a *bias vector* b_i to the result of step 1.
3. Apply the (usually) nonlinear *activation function* $a(x)$.

Mathematically, this corresponds to

$$c_i^{(l+1)} = a \left[\left(\sum_{j=1}^N w_{ij}^{(l)} c_j^{(l)} \right) + b_i^{(l)} \right]. \quad (2)$$

This is done layer by layer, starting from the input layer and ending in the output layer. For simplicity, every neuron in a layer is assigned the same activation function. Although this limits the generality in the function space accessible to the NN, it increases the numerical stability of the optimizer. In the present case, we chose $a(z) = \tanh(z)$ for some input z for all nodes except those in the last layer for which a linear activation function is required.

The so called *loss* or *cost function* gives a measure of the quality of the NN. For simplicity, we contract the multiple input features and output labels into an input vector $\boldsymbol{\gamma}^i \equiv (\mathbf{y}, \mathbf{v}_y, t)^T$ and an output vector $\tilde{\boldsymbol{\gamma}}^o(\boldsymbol{\gamma}^i) \equiv (\tilde{x}, \tilde{v}_x)^T$, respectively. We use the mean squared error as the loss function

$$C_{\mathbf{w}, \mathbf{b}}(\boldsymbol{\gamma}^o, \tilde{\boldsymbol{\gamma}}^o) = \frac{1}{2n} \sum_{i=1}^n \|\boldsymbol{\gamma}_i^o - \tilde{\boldsymbol{\gamma}}^o(\boldsymbol{\gamma}_i^i)\|^2, \quad (3)$$

for the n examples in the *test data* or *training data* of points in space and time of the NHIM. The data set $\{\boldsymbol{\gamma}_i^i, \boldsymbol{\gamma}_i^o\}$ with $i \in [1, n]$ is obtained with the binary contraction method mentioned above and described in Refs. 36 and 60. The subscripts \mathbf{w}, \mathbf{b} indicate the dependence on the weight matrices and the bias vectors.

During the training of the NN the weights, i.e., the values of the weight matrices and the bias vectors, are adjusted such that the loss given in Eq. (3) is minimized. In our case, this is done by a modified version of *stochastic gradient descent* [63], which is called an *Adam optimizer* [64]. The learning rate η , determining the step size of the gradient descent method, is set to $\eta = 0.1$ and all other optimizer parameters are in accordance to the original publication [64]. In comparison to previous works like Ref. 59, this simplifies the choice of hyper-parameters. The NN and its optimization is implemented using the *Python* library *Tensorflow* [65]. All NNs implemented here have three neurons in the input layer, two neurons in the output layer, and three hidden layers with 100, 100, and 40 neurons, respectively in order.

An aim of this paper is to use NNs to effect a multidimensional regression task. In particular, for d -dimensional systems we need a continuous description of the $(2d - 2)$ -dimensional NHIM that is embedded in the $(2d + 1)$ -dimensional *extended phase space* (phase space plus time). We use $2d - 2$ phase space coordinates \mathbf{y}, \mathbf{v}_y and the time t as input vectors and obtain the corresponding two phase space coordinates (x, v_x) on the NHIM, see Eq. (1) and Fig. 1(a). The training data can be generated as described above using the binary contraction method [36, 60]. Training was done with 50 000 training points over 50 000 epochs, which took about 2 hours of computational time on an *Intel(R) Core(TM) i5-3470 CPU* with 3.20 GHz.

In comparison to the direct application of the binary contraction, the NN takes a factor of 200 less in computational time. It suffers a reduction in precision from about 10^{-15} (for the binary contraction method) to about 10^{-4} (for the NN). However, the stabilization of the dynamics on the NHIM does not require very high precision, as will be discussed in Sec. IIIB. Alternative machine learning methods like Gaussian Process Regression (GPR) could be used as well. However, due to the relative high number of trainings points (about 50 000) that are needed for the required accuracy, inferring of GPR would be expected to be slower than the NN in this case. More details are given in Ref. 36. We anticipate that future work could perhaps obtain improved efficiency by optimizing the NNs through advances in machine learning techniques. However, this would not alter the physical interpretation of the present results.

B. Stabilization of trajectories on the NHIM

Due to the unstable degree of freedom, trajectories tend to move away from the NHIM. The distance be-

tween the orbit and the NHIM increases exponentially fast in time, and thus the initial conditions of a trajectory must be known with numerically inaccessible precision to keep it on the NHIM for long times. This makes a long-time analysis of the dynamics on the NHIM extremely difficult or even impossible.

Here, we present a method for stabilizing the motion of trajectories on the NHIM. In Sec. II A we have shown that a NN can be used to describe the $(2d - 2)$ -dimensional NHIM. Here we apply this NN to guide the trajectory on the unstable manifold, i.e., to correct any deviation from the NHIM during the numerical integration of the orbit. The procedure is as follows: Using the NN, we choose an arbitrary initial point on the NHIM. Note that the uncertainty of the initial conditions is determined by the numerical accuracy of the NN. From this point, the trajectory is propagated for a small time step. This numerical step may have naively increased the distance between the trajectory and the NHIM. We assume that this deviation is manifested mainly in the reaction coordinate x and the corresponding velocity v_x , indicating the falloff of the trajectory from the NHIM along the unstable direction. It is thus necessary to guide the trajectory back to the NHIM. We achieve this by replacing the calculated position $x(t)$ of the reaction coordinate and the corresponding velocity $v_x(t)$, which may slightly deviate from the NHIM, with the (numerically) exact values, x and v_x , on the NHIM given by the NN based on the data set of points from Eq. (1). The error here is limited, as discussed in Sec. II A, because the error of the NN itself is small compared to the exponential increase of the deviation along the unstable reaction coordinate in time without the stabilization. By repeating this procedure after each time step, we prevent the trajectory from leaving the NHIM. Note that this procedure is not limited to systems with two degrees of freedom and can be applied for any dimension of the problem as long as the data base feeding the NN sufficiently spans the underlying domain of $(\mathbf{y}, \mathbf{v}_y, t)$. Furthermore, this construction does not require (and is not restricted to) either the trajectories or the external driving to be periodic in time as assumed in the illustrative examples below.

For the special case of a periodically driven system with $d = 2$ degrees of freedom, discussed in Sec. III, the stabilization restricts the dynamics of the trajectories from the $(4 + 1)$ -dimensional extended phase space (including time) of $H(x, v_x, y, v_y, t)$, as discussed in Ref. 36, to the $(2 + 1)$ -dimensional subspace of the NHIM, viz.

$$\begin{aligned} & H(x^{\text{NHIM}}(y, v_y, t), v_x^{\text{NHIM}}(y, v_y, t), y, v_y, t) \\ &= H^{\text{NHIM}}(y, v_y, t). \end{aligned} \quad (4)$$

This is effectively a periodically driven one degree of freedom system. As such, it can in principle show regular, chaotic or mixed regular-chaotic dynamics [66]. The dynamics can be visualized using a Poincaré surface of section (PSOS) with a stroboscopic map for time, i.e., points $(y(t), v_y(t))$ are drawn at times $t = t_B + nT$ with t_B the barrier phase, T the period of the driving, and $n \in \mathbb{N}$.

The analysis of the PSOS allows one to deduce the dynamics of the system from structures of the trajectories in the NHIM. In particular, periodic orbits appear as fixed points. Linear structures in the PSOS indicate the existence of exact or approximate constants of motion and thus regular dynamics. Chaotic dynamics is related to the breakdown of constants of motion and is visualized as stochastic regions in the PSOS [67].

A fixed point with period one in the PSOS indicates a periodic orbit with the same period as the driving potential. In analogy to systems with one degree of freedom [37–46] we define this orbit as the TS trajectory. It is of major importance for the following reasons. In dissipative, non-periodic systems the TS trajectory is the unique trajectory that is bound to the vicinity of the saddle for all times [37, 38, 46]. In Hamiltonian systems, the TS trajectory has, at least qualitatively, only the minimal amount of the (in driven systems not conserved) energy that is necessary to follow the saddle motion and the least energy for motion in additional directions. It is therefore located in the low energy regime of the barrier. This holds also for trajectories in dissipative systems, since their additional energy is damped with time. Trajectories in the low energy regime of the barrier are assumed to be strongly influenced by the saddle. On the other hand, the TS trajectory allows for the calculation of the reaction rate by an alternative method, to the often used ensemble propagation [42, 43].

C. Rate constants

As mentioned above, the NHIM is of particular importance because the dynamics close to this manifold determines the rate constants of trajectories crossing the saddle region. Rate constants can be computed by propagating a large ensemble of trajectories starting close to the dividing surface (DS) and subsequently fitting the number of trajectories $N_{\text{react}}(t)$ that remain reactants over time before crossing the moving DS to the exponential form

$$N_{\text{react}}(t) - N_{\infty} \propto \exp(-kt) \quad (5)$$

where k is the resulting rate constant. Details are given in Refs. 35 and 36.

For systems with one degree of freedom, a computationally less expensive method for obtaining rate constants has been derived by Craven et al. [42]. Here, we give a short review of this method, which is based on the Floquet analysis of the TS trajectory.

For simplicity we generalize the configuration space coordinates x_i (for the i -th degrees of freedom, in a system with d degrees of freedom) and the momentum coordinates p_i to the phase space coordinates

$$\boldsymbol{\gamma} = (x_1, x_2, \dots, x_d, p_1, \dots, p_d)^{\text{T}}. \quad (6)$$

With this notation the equations of motion transform to

$$\dot{\gamma} = \mathbf{J} \frac{\partial H}{\partial \gamma} \quad \text{with} \quad \mathbf{J} = \begin{pmatrix} \mathbf{0}_d & \mathbf{1}_d \\ -\mathbf{1}_d & \mathbf{0}_d \end{pmatrix}, \quad (7)$$

where H denotes the Hamiltonian of the system, and $\mathbf{1}_d$ and $\mathbf{0}_d$ describe the d -dimensional identity and zero matrix, respectively. Based on this, the *stability* or *monodromy matrix* for a trajectory starting at $\gamma(0)$ is defined according to [68]

$$\mathbf{M}_{ij}[\gamma(0), t] = \frac{\partial \gamma_i(t)}{\partial \gamma_j(0)}. \quad (8)$$

By considering two initially neighboring trajectories, it follows by chain rule from Eqs. (7) and (8) the differential equation

$$\dot{\mathbf{M}} = \mathbf{J} \frac{\partial^2 H}{\partial \gamma^2} \mathbf{M}, \quad \mathbf{M}(0) = \mathbf{1}_{2d}. \quad (9)$$

For Hamiltonian systems, i. e. in systems without friction, the monodromy matrix \mathbf{M} is symplectic. This means, if λ is an eigenvalue of \mathbf{M} then $1/\lambda$ and their complex conjugates $\bar{\lambda}$, $1/\bar{\lambda}$ are also eigenvalues. Since the monodromy matrix has only real entries, the eigenvalues are either complex conjugated or inverse to each other.

In the following m_1 denotes the larger eigenvalue and $m_s = 1/m_1$ denotes the smaller one. For periodic trajectories with period T , the so called *Floquet exponents* are defined by

$$\mu_{1,s} = \frac{1}{T} \ln |m_{1,s}|. \quad (10)$$

An important fact about the Floquet exponents is that they correspond to the rate at which two neighboring trajectories separate from each other [68]. Eigenvalues with absolute value equal to one correspond to vanishing Floquet exponents. Hence, neighboring trajectories do not separate exponentially. This corresponds to a stable degree of freedom. On the other hand, eigenvalues with absolute value unequal to one correspond to non-vanishing Floquet exponents and therefore to an unstable degree of freedom. Thus, in a one-dimensional system the reaction rate constant is determined by the two Floquet exponents of the TS trajectory and follows from Ref. 42 as

$$k_{\text{Floquet}} = \mu_1 - \mu_s. \quad (11)$$

III. RESULTS AND DISCUSSION

We now benchmark the methods described above using a system with non-trivial dynamics—i. e. one that contains a mix of regular and chaotic behavior [66]—on a time-dependent NHIM. Such behavior arises readily in nonlinear coupled multidimensional systems with high dimensionality. Indeed, most chemical reactions have such

a structure. Nevertheless, for relative simplicity, we consider a low-dimensional time-dependent model reaction which admits detailed analysis while retaining the requisite complexity. Further requirements to the model system are the existence of a rank-1 saddle and a periodic oscillation in the saddle's position.

A. Model System

The two-dimensional model system from Ref. 35 with the time-dependent potential

$$V(x, y, t) = E_b \exp\left(-\alpha [x - \hat{x} \sin(\omega_x t)]^2\right) + \frac{\omega_y^2}{2} \left[y - \frac{2}{\pi} \arctan(2x)\right]^2 \quad (12)$$

satisfies our requirements for verifying the accuracy of the approach through a nontrivial example. It contains a Gaussian barrier with height E_b and width a , and oscillates along the x axis with frequency ω_x and amplitude \hat{x} . It is bound along the y direction through a harmonic potential with frequency ω_y , and is nonlinearly coupled to the minimum energy path x through a term proportional to $y \arctan(2x)$. For simplicity, all variables are dimensionless and in accordance to Ref. 35 set to $E_b = 2$, $\alpha = 1$, $\omega_x = \pi$, and $\omega_y = 2$. The amplitudes \hat{x} of the oscillations in the saddle range between 0 and 0.8.

B. Dynamics on the NHIM

To visualize trajectories we use Poincaré surfaces of section as trajectories cut through the y and v_y plane. This works well in the current case of a time-dependent and periodically driven system because the response of the system is similarly periodic. Consequently, a stroboscopic representation taken at intervals matching the period of the driving, such as that shown in Fig. 2, provides a view of stable structures, such as the tori, or unstable ones, if they appear in the system.

The trajectories shown in the stroboscopic view in Fig. 2 were sampled around the TS trajectory, which is obtained by an algorithm that is described later. It is remarkable that all trajectories approximately lie on ellipses, meaning that the phase space contains stable tori. This implies that there is an approximately conserved quantity for a fixed barrier phase [69]. In other words, the system shows regular behavior. It is robust to changes in the oscillation amplitude as we found it to persist at various values, i. e., $\hat{x} = 0.0, 0.1, \text{ or } 0.8$. Consequently, these systems are near-integrable in the regime close to the rank-1 saddle. This does not necessarily hold for regimes far from the saddle or for arbitrary system parameters.

As mentioned before, we want to localize the TS trajectory in a periodically driven system. In the PSOS,

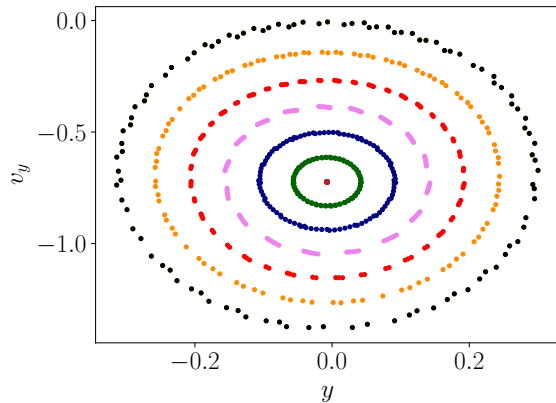


FIG. 2. Poincaré surface of section (PSOS) of the system (12) with amplitude $\hat{x} = 0.4$ using a stroboscopic map with barrier phase $t_B = 0$. Trajectories with various initial conditions have been stabilized on the NHIM via a NN and propagated for 100 periods of the driving potential. The fixed point at the center of the regular torus-like structures marks the TS trajectory.

the TS trajectory should appear as a fixed point in the stroboscopic view because the periodicity of the trajectory is equal to that of the driven barrier motion. In the following, we present two algorithms for finding a point on the TS trajectory from which the trajectory itself can be obtained by using the stabilization via a NN.

The first algorithm, which we call *centroid search* uses the fact, that we have a periodic system, so the potential is identical after a full period in time has passed. Note that the PSOS in Fig. 3 is given for a fixed barrier phase $t_B = 0$. The result is shown in a stroboscopic view in Fig. 3(a). The iterations of the first initial point, marked with a “1” lead to the red dots. The centroid or geometric center of these points is the green asterisk marked with a “2” and is the initial point of the next trajectory. The next iteration yields the initial point “3” and the blue plus symbols. As can be seen, the algorithm converges rapidly to a fixed point for the particular barrier phase plotted. This means that the trajectory period is equal to the system period. For all investigated initial coordinates, the algorithm converged to the same trajectory which is the only one that has a periodicity equal to the system periodicity. Therefore it is in accordance to the definition in Sec. IIB and must be a periodic TS trajectory. Fig. 3(a) also shows that the centroid search converges within a small number of iterations and is thereby computationally inexpensive.

The centroid search algorithm is restricted to periodically driven systems because it requires a stroboscopic view. To overcome this problem, we developed a second algorithm. We will once again take advantage of the TS trajectory which has thus far been seen in this work as a fixed point of the stroboscopic map in the context of periodic systems. In non-periodic systems, a TS trajectory is known to be a trajectory bound to the vicinity of the

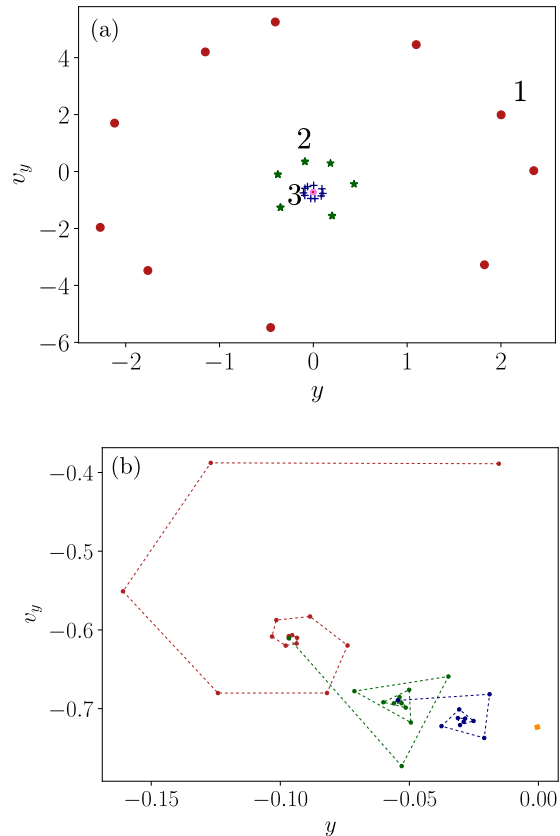


FIG. 3. (a) Centroid search for the TS trajectory of system (12) with $\hat{x} = 0.4$. Stroboscopic view of trajectories for 10 periods determined using stabilization generated with a NN. Three selected initial points of trajectories are marked as 1, 2 and 3, and correspond to the stroboscoped points marked as blue red dots, green stars and blue crosses, respectively. The centroid of the n^{th} trajectory corresponds to the initial point of the $(n + 1)^{\text{st}}$ trajectory, e.g. point 2 is the centroid of the red points of trajectory 1. The algorithm converges to the TS trajectory, located, for the given barrier phase $t_B = 0$, at $y \approx 0.00$, $v_y \approx -0.72$. (b) Friction search for the TS trajectory. The algorithm starts with large friction (red line) for the TS trajectory starting point. The trajectory forms a spiral, starting in the upper right corner and converging to a point that is closer to a periodic TS trajectory than the initial point. During the propagation of the particle the friction was reduced twice (green and blue line). The initial point of the green curve corresponds to the final point of the red curve. The orange dot marks the point to which the friction search finally converges by successively reducing the friction. Details of both algorithms are given in the text.

saddle for all time.

The second algorithm, which we call *friction search*, relies on the introduction of an auxiliary friction that reduces the energy of an arbitrary trajectory on the NHIM. The latter converges to that specific trajectory with the lowest possible energy on the NHIM. High friction in the algorithm leads to a fast convergence, since the energy

TABLE I. Eigenvalues m and Floquet exponents μ of the periodic TS trajectory (determined with centroid search) for the potential barrier amplitude $\hat{x} = 0.4$.

m	μ
44.98	+1.903
0.02223	-1.903
$0.4373 + 0.8993i$	0
$0.4373 - 0.8993i$	0

dissipation is high, but the error in determining the TS trajectory is large. This can be seen in Fig. 3(b). Low friction decreases the convergence speed but increases the precision. Therefore we start with a large friction at an arbitrary point (red curve in Fig. 3(b)) and propagate until the trajectory converges. Then the friction coefficient is decreased and the prior convergence point is used as the new initial point of the propagation. Propagation and friction coefficient reduction is done iteratively (green and blue curves in Fig. 3(b)) to get a precise TS trajectory starting point. Fig. 3(b) shows that the friction search converges to a similar value as the centroid search, which is marked by an orange dot. The slow energy dissipation for small friction is the reason why friction search converges slower than the centroid search, however, this second method should work reliably in systems with many degrees of freedom, and for arbitrary driving.

C. Analysis of the TS trajectory and rate constants

In this section we use the point on a periodic TS trajectory determined by the centroid search to obtain this TS trajectory itself. We obtain the latter by using either a conventional numerical integrator or the stabilization on the NHIM via an NN. The results are shown through a non stroboscopic view in Fig. 4(a). There is great agreement between the two different trajectories during at least the first period. The distance in the x -direction between the two trajectories reported in Fig. 4(b) shows nearly exponential separation. This is due to the fact that the unstable degree of freedom of the rank-1 saddle causes the trajectory, which is close to the NHIM but not directly on the NHIM, to increasingly deviate from the latter. Significantly, the agreement in the trajectories during the first period seen in Fig. 4b confirms that the modification (i) does not change the underlying physical behavior of the trajectory and (ii) prevents the trajectory from leaving its perfect periodic orbit.

The stabilized trajectory (black line in Fig. 4(a)) is used for the Floquet analysis in the following. Table I shows the eigenvalues m of the monodromy matrix and Floquet exponents $\mu = (1/T) \ln |m|$ (with T describing the period time) of the periodic TS trajectory. It can be seen that the two real eigenvalues are inverse to each other and the two complex ones are complex conjugated.

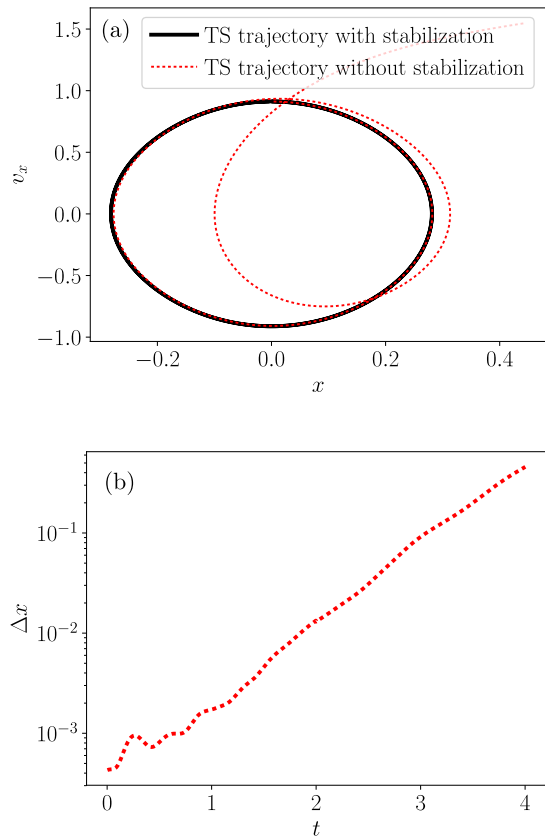


FIG. 4. (a) Projection of the TS trajectory, determined by the centroid search. Trajectories are plotted over 2.5 periods for both, the trajectory determination with and without the stabilization on the NHIM. (b) Distance Δx between the x -coordinates of the two trajectories calculated with and without the stabilization over two periods. Within one period the separation is two orders of magnitudes smaller than the actual motion in x direction.

TABLE II. Reaction rate constants k obtained by Floquet analysis of the TS trajectories and by ensemble propagation for different barrier oscillation amplitudes \hat{x} .

\hat{x}	k_{Floquet}	k_{Ensemble}
0.0	2.761	2.762
0.1	2.979	3.020
0.4	3.806	3.804
0.8	4.016	3.994

This shows that the monodromy matrix of our TS trajectory is indeed symplectic, which is in agreement with the theory.

The aforementioned Floquet exponents yield via Eq. (11) the corresponding reaction rate constant, e.g., $k_{\text{Floquet}} = 3.806$ for the model system (12) with barrier amplitude $\hat{x} = 0.4$. The same analysis is done for three other sets of system parameters ($\hat{x} = 0.0, 0.1, 0.8$) and the results are shown in Table II. For comparison,

the reaction rates were also computed by observing the population decay of an ensemble of trajectories, and the resulting rates are listed in the second column of Table II. The agreement is excellent. It provides further verification of the earlier conjecture of Craven et al. [43] stated in Eq. (11) for obtaining rates directly from the geometric stability (and instability) of the TS trajectory. Calculating the reaction rates with the Floquet method is about two orders of magnitudes faster in computational time than the ensemble method. This relies on the fact that ensembles require the calculation of millions of trajectories, while only single trajectories need to be considered in the Floquet method.

IV. CONCLUSION AND OUTLOOK

In this paper, we have applied neural networks (NNs) to describe the normally hyperbolic invariant manifolds (NHIMs) of periodically driven multidimensional systems with a rank-1 saddle. Use of these NNs allows for the efficient propagation of stabilized trajectories on the NHIM with respect to the unstable degrees of freedom of a rank-1 barrier even for longer integration times. Without such stabilization, these trajectories would depart exponentially fast from the NHIM to either the reactant or the product side due to the limited precision of numerical calculations, as seen in in Ref. 36. It enables the analysis of the long-time dynamics on the NHIM using a stroboscopic Poincaré surface of section (PSOS). Therein, fixed points can be determined by two different methods, viz. the centroid search and the friction search. The application of the NN-enabled approaches to a model system with two degrees of freedom reveals the existence of near-integrable tori surrounding a periodic transition state (TS) trajectory given by a period one fixed point of the Poincaré map.

The rate constants of the system obtained from the propagation of large trajectory ensembles are in excellent

agreement with the rates obtained by a Floquet analysis associated with the periodic TS trajectory extended and applied to a periodic TS trajectory of the higher-dimensional system. In Ref. 42 this analysis was applied to the periodic TS trajectory of a *one*-dimensional system, which coincides with the NHIM. Here, we have generalized this method to any periodic trajectory on the NHIM of a *multidimensional* rank-1 saddle.

While the model system shows regular dynamics on the NHIM, it remains for future work to investigate whether a transition from regular to chaotic dynamics can be observed, e.g., when changing the amplitude and frequency of the moving saddle. It will also be challenging to study rate constants for trajectories crossing the dividing surface (DS) not close to the periodic TS trajectory but in other regions of phase space.

Finally, the methods introduced in this paper should be applied to other more realistic multidimensional systems, like the LiCN \leftrightarrow LiNC [70] or the ketene [71] isomerization reactions, and further extended to systems with thermal activation or friction.

ACKNOWLEDGMENTS

The German portion of this collaborative work was supported by Deutsche Forschungsgemeinschaft (DFG) through Grant No. MA1639/14-1. RH's contribution to this work was supported by the National Science Foundation (NSF) through Grant No. CHE-1700749. MF is grateful for support from the Landesgraduiertenförderung of the Land Baden-Württemberg. This collaboration has also benefited from support by the European Union's Horizon 2020 Research and Innovation Program under the Marie Skłodowska-Curie Grant Agreement No. 734557. The machine learning framework *Tensorflow* has been used to train the neural networks [65].

-
- [1] K. S. Pitzer, F. T. Smith, and H. Eyring, *The Transition State*, Special Publ. (Chemical Society, London, 1962) p. 53.
 - [2] P. Pechukas, *Annu. Rev. Phys. Chem.* **32**, 159 (1981).
 - [3] B. C. Garrett and D. G. Truhlar, *J. Phys. Chem.* **83**, 1052 (1979).
 - [4] D. G. Truhlar, A. D. Issacson, and B. C. Garrett, "Theory of chemical reaction dynamics," (CRC Press, Boca Raton, FL, 1985) pp. 65–137.
 - [5] J. T. Hynes, *Annu. Rev. Phys. Chem.* **36**, 573 (1985).
 - [6] B. J. Berne, M. Borkovec, and J. E. Straub, *J. Phys. Chem.* **92**, 3711 (1988).
 - [7] A. Nitzan, *Adv. Chem. Phys.* **70**, 489 (1988).
 - [8] P. Hänggi, P. Talkner, and M. Borkovec, *Rev. Mod. Phys.* **62**, 251 (1990), and references therein.
 - [9] G. A. Natanson, B. C. Garrett, T. N. Truong, T. Joseph, and D. G. Truhlar, *J. Chem. Phys.* **94**, 7875 (1991).
 - [10] D. G. Truhlar, B. C. Garrett, and S. J. Klippenstein, *J. Phys. Chem.* **100**, 12771 (1996).
 - [11] D. G. Truhlar and B. C. Garrett, *J. Phys. Chem. B* **104**, 1069 (2000).
 - [12] T. Komatsuzaki and R. S. Berry, *Proc. Natl. Acad. Sci. U.S.A.* **98**, 7666 (2001).
 - [13] E. Pollak and P. Talkner, *Chaos* **15**, 026116 (2005).
 - [14] H. Waalkens, R. Schubert, and S. Wiggins, *Nonlinearity* **21**, R1 (2008).
 - [15] T. Bartsch, J. M. Moix, R. Hernandez, S. Kawai, and T. Uzer, *Adv. Chem. Phys.* **140**, 191 (2008).
 - [16] S. Kawai and T. Komatsuzaki, *Phys. Rev. Lett.* **105**, 048304 (2010).
 - [17] R. Hernandez, T. Bartsch, and T. Uzer, *Chem. Phys.* **370**, 270 (2010).
 - [18] O. Sharia and G. Henkelman, *New J. Phys.* **18**, 013023 (2016).

- [19] C. Jaffé, D. Farrelly, and T. Uzer, *Phys. Rev. Lett.* **84**, 610 (2000).
- [20] G. Jacucci, M. Toller, G. DeLorenzi, and C. P. Flynn, *Phys. Rev. Lett.* **52**, 295 (1984).
- [21] T. Komatsuzaki and R. S. Berry, *J. Chem. Phys.* **110**, 9160 (1999).
- [22] T. Komatsuzaki and R. S. Berry, *Adv. Chem. Phys.* **123**, 79 (2002).
- [23] M. Toller, G. Jacucci, G. DeLorenzi, and C. P. Flynn, *Phys. Rev. B* **32**, 2082 (1985).
- [24] A. F. Voter, F. Montalenti, and T. C. Germann, *Annu. Rev. Mater. Res.* **32**, 321 (2002).
- [25] H. P. de Oliveira, A. M. Ozorio de Almeida, I. Damiaão Soares, and E. V. Tonini, *Phys. Rev. D* **65**, 083511/1 (2002).
- [26] C. Jaffé, S. D. Ross, M. W. Lo, J. Marsden, D. Farrelly, and T. Uzer, *Phys. Rev. Lett.* **89**, 011101 (2002).
- [27] H. Waalkens, A. Burbanks, and S. Wiggins, *Mon. Not. R. Astron. Soc.* **361**, 763 (2005).
- [28] C. Huepe, S. Métens, G. Dewel, P. Borckmans, and M. E. Brachet, *Phys. Rev. Lett.* **82**, 1616 (1999).
- [29] C. Huepe, L. S. Tuckerman, S. Métens, and M. E. Brachet, *Phys. Rev. A* **68**, 023609 (2003).
- [30] A. Junginger, J. Main, G. Wunner, and M. Dorwarth, *J. Phys. A: Math. Theor.* **45**, 155201 (2012).
- [31] A. Junginger, M. Dorwarth, J. Main, and G. Wunner, *J. Phys. A: Math. Theor.* **45**, 155202 (2012).
- [32] A. Junginger, M. Kreibich, J. Main, and G. Wunner, *Phys. Rev. A* **88**, 043617 (2013).
- [33] C. Mendoza and A. M. Mancho, *Phys. Rev. Lett.* **105**, 038501 (2010).
- [34] A. M. Mancho, S. Wiggins, J. Curbelo, and C. Mendoza, *Commun. Nonlinear Sci. Numer. Simul.* **18**, 3530 (2013).
- [35] M. Feldmaier, A. Junginger, J. Main, G. Wunner, and R. Hernandez, *Chem. Phys. Lett.* **687**, 194 (2017).
- [36] M. Feldmaier, P. Schraft, R. Bardakcioglu, J. Reiff, M. Lober, M. Tschöpe, A. Junginger, J. Main, T. Bartsch, and R. Hernandez, *J. Phys. Chem. B* **123**, 2070 (2019).
- [37] T. Bartsch, R. Hernandez, and T. Uzer, *Phys. Rev. Lett.* **95**, 058301 (2005).
- [38] T. Bartsch, T. Uzer, and R. Hernandez, *J. Chem. Phys.* **123**, 204102 (2005).
- [39] T. Bartsch, T. Uzer, J. M. Moix, and R. Hernandez, *J. Chem. Phys.* **124**, 244310 (2006).
- [40] S. Kawai and T. Komatsuzaki, *J. Chem. Phys.* **131**, 224505 (2009).
- [41] G. T. Craven, T. Bartsch, and R. Hernandez, *Phys. Rev. E* **89**, 040801(R) (2014).
- [42] G. T. Craven, T. Bartsch, and R. Hernandez, *J. Chem. Phys.* **141**, 041106 (2014).
- [43] G. T. Craven, T. Bartsch, and R. Hernandez, *J. Chem. Phys.* **142**, 074108 (2015).
- [44] A. Junginger and R. Hernandez, *J. Phys. Chem. B* **120**, 1720 (2016).
- [45] A. Junginger, G. T. Craven, T. Bartsch, F. Revuelta, F. Borondo, R. M. Benito, and R. Hernandez, *Phys. Chem. Chem. Phys.* **18**, 30270 (2016).
- [46] A. Junginger and R. Hernandez, *Phys. Chem. Chem. Phys.* **18**, 30282 (2016).
- [47] S. Kawai, H. Teramoto, C.-B. Li, T. Komatsuzaki, and M. Toda, “Dynamical reaction theory based on geometric structures in phase space,” in *Advancing Theory for Kinetics and Dynamics of Complex, Many-Dimensional Systems: Clusters and Proteins* (Wiley-Blackwell, 2011) pp. 123–169.
- [48] B. K. Carpenter, G. S. Ezra, S. C. Farantos, Z. C. Kramer, and S. Wiggins, *J. Phys. Chem. B* **122**, 3230 (2018).
- [49] T. B. Blank, S. D. Brown, A. W. Calhoun, and D. J. Doren, *J. Chem. Phys.* **103**, 4129 (1995).
- [50] J. Behler and M. Parrinello, *Phys. Rev. Lett.* **98**, 146401 (2007).
- [51] J. Behler, *J. Chem. Phys.* **134**, 074106 (2011).
- [52] J. Cui and R. V. Krems, *J. Phys. B* **49**, 224001 (2016).
- [53] R. A. Vargas-Hernández, Y. Guan, D. H. Zhang, and R. V. Krems, *New J. Phys.* **21**, 022001 (2019).
- [54] M. Rupp, A. Tkatchenko, K.-R. Müller, and O. A. von Lilienfeld, *Phys. Rev. Lett.* **108**, 058301 (2012).
- [55] J. Cui and R. V. Krems, *Phys. Rev. Lett.* **115**, 073202 (2015).
- [56] J. Cui, Z. Li, and R. V. Krems, *J. Chem. Phys.* **143**, 154101 (2015).
- [57] F. A. Faber, A. Lindmaa, O. A. von Lilienfeld, and R. Armiento, *Phys. Rev. Lett.* **117**, 135502 (2016).
- [58] B. Huang and O. A. von Lilienfeld, arXiv preprint arXiv:1707.04146 (2017).
- [59] P. Schraft, A. Junginger, M. Feldmaier, R. Bardakcioglu, J. Main, G. Wunner, and R. Hernandez, *Phys. Rev. E* **97**, 042309 (2018).
- [60] R. Bardakcioglu, A. Junginger, M. Feldmaier, J. Main, and R. Hernandez, *Phys. Rev. E* **98**, 032204 (2018).
- [61] I. Goodfellow, Y. Bengio, and A. Courville, *Deep Learning* (MIT Press, 2016) <http://www.deeplearningbook.org>.
- [62] M. A. Nielsen, *Neural Networks and Deep Learning* (Determination Press, 2015) <http://neuralnetworksanddeeplearning.com/>.
- [63] H. Robbins and S. Monro, *The Annals of Mathematical Statistics* **22**, 400 (1951).
- [64] D. P. Kingma and J. Ba, *CoRR* **abs/1412.6980** (2014).
- [65] M. Abadi, A. Agarwal, P. Barham, E. Brevdo, Z. Chen, C. Citro, G. S. Corrado, A. Davis, J. Dean, M. Devin, S. Ghemawat, I. Goodfellow, A. Harp, G. Irving, M. Isard, Y. Jia, R. Jozefowicz, L. Kaiser, M. Kudlur, J. Levenberg, D. Mané, R. Monga, S. Moore, D. Murray, C. Olah, M. Schuster, J. Shlens, B. Steiner, I. Sutskever, K. Talwar, P. Tucker, V. Vanhoucke, V. Vasudevan, F. Viégas, O. Vinyals, P. Warden, M. Wattenberg, M. Wicke, Y. Yu, and X. Zheng, (2015), software available from tensorflow.org.
- [66] H. Breuer, K. Dietz, and M. Holthaus, *Physica D: Nonlinear Phenomena* **46**, 317 (1990).
- [67] A. J. Lichtenberg and M. A. Leibermann, *Regular and Stochastic Motion* (Springer, New York, 1982).
- [68] H. Goldstein, *Classical mechanics*, Addison-Wesley series in physics (Addison-Wesley, 1980).
- [69] S. Wimberger, *Nonlinear Dynamics and Quantum Chaos* (Springer International Publishing, 2014).
- [70] A. Junginger, P. L. Garcia-Muller, F. Borondo, R. M. Benito, and R. Hernandez, *J. Chem. Phys.* **144**, 024104 (2016).
- [71] G. T. Craven and R. Hernandez, *Phys. Chem. Chem. Phys.* **18**, 4008 (2016).